Novel instrument for surface plasmon polariton tracking in space and time

M. Sandtke, R. J. P. Engelen, H. Schoenmaker, I. Attema, H. Dekker, I. Cerjak,
J. P. Korterik,[a)] F. B. Segerink,[a)] and L. Kuipers[b)]
*FOM Institute for Atomic and Molecular Physics (AMOLF), Kruislaan 407, 1098 SJ Amsterdam,
TheNetherlands*

We describe the realization of a phase-sensitive and ultrafast near-field microscope, optimized for investigation of surface plasmon polariton propagation. The apparatus consists of a homebuilt near-field microscope that is incorporated in Mach-Zehnder-type interferometer which enables heterodyne detection. We show that this microscope is able to measure dynamical properties of both photonic and plasmonic systems with phase sensitivity. © *2008 American Institute of Physics.*
[DOI: 10.1063/1.2825463]

I. INTRODUCTION

Surface plasmon polaritons (SPPs), which are the solution of Maxwell's equations at the interface between a dielectric and a metal,[1,2] have captured the interest of scientists from a wide range of disciplines. For instance, SPPs are being explored for applications in merging optics and electronics[3] data storage,[4] improving conventional microscopy[5] and solar cells.[6] Already they are used in sensors for detecting biologically interesting molecules.[7,8] Most of these applications require SPP propagation and manipulation on a micrometer, or even submicrometer scale. SPP properties at these length scales are not easy to model. Therefore, a measurement technique able investigate SPP behavior on a (sub)micrometer scale is very valuable. For a complete picture of the SPP behavior, at every position along a SPP device, one would like to know the amplitude and phase of the SPP E-field. In order to investigate the dynamical behavior of SPPs, time-resolved measurements are also required.

The SPPs are bound to a metal-dielectric interface, which makes it complicated to detect them. Imaging their propagation with far-field optics will only work if the SPPs are coupled back to photons first. Four main methods have been reported in literature to detect SPPs. The first method is to detect the leakage radiation.[9] Roughness will scatter SPPs into far-field radiation (photons) that can be detected with a microscope. Drawback of this technique is that one measures the scattered field, rather than the SPP itself, i.e., the scatterer is an integral part of the detected field. The second technique uses fluorescent probes such as dye molecules[10] or Er^{3+} ions.[11] For sufficiently low concentrations the probes do not perturb the SPP under investigation, so with this technique one can visualize the bound mode. However, diffraction will limit the resolution of this technique and all phase and time information is lost. The third technique to detect SPPs is by

photoelectron emission microscopy (PEEM).[12] This technique obtained time and phase sensitivity for SPPs on a grating[13] and a smooth metal film[14] with a subwavelength resolution. An actual movie was presented showing SPP propagation with <10 fs temporal resolution using PEEM.[14] Unfortunately, PEEM requires (ultra) high vacuum conditions at the sample, which can hinder experiments. Also this technique cannot be used to study photonic systems like photonic crystals. Another technique to study SPP dynamics is by optical pump-probe experiments.[15] Using this technique the authors of Ref. 15 were able to determine the SPP dephasing and found a momentum lifetime of 48 fs. While pump probe is a very useful technique for time-resolved experiments, it is generally not a phase-resolved technique.

The most common method for studying SPP propagation is by using a near-field microscope,[16] or a photon scanning tunneling microscope (PSTM). In literature results have been shown of near-field measurements on (guided) SPPs.[17–21] These papers show the SPP Bloch behavior on a SPP grating,[17] and a full investigation of the near-field distribution of SPPs guided by a metal guide.[18] The influence of the width of the metal guide was examined in terms of mode profile[19] and waveguide cutoff.[20] All these investigations, with the exception of Ref. 21, measure time-averaged intensity distributions. In this paper we present a near-field microscope to study SPP behavior with both amplitude and phase information of the SPP E-field. It also allows time-resolved measurements to study SPP dynamics.

This paper is organized as follows: first the microscope requirements are listed in Sec. II. The realized instrument is described in Sec. III. Sections IV and V describe the theoretical background of the measurements. In Secs. V A and V B the two different measurement schemes possible with the instrument are presented. Experimental results are given in Sec. VI.

---

a)Optical Science Group, MESA+ Research Institute and Department of Science Technology, University of Twente, P.O. Box 217, 7500 AE Enschede, The Netherlands.
b)Electronic mail: l.kuipers@amolf.nl.

A. Surface plasmon polariton excitation

The dispersion of SPPs on a smooth metal surface is given by

$$k_{SPP} = \frac{\omega}{c}\left(\frac{\epsilon_m \epsilon_d}{\epsilon_m + \epsilon_d}\right)^{1/2}, \qquad (1)$$

here k_{SPP} is the SPP wavevector, c the speed of light in vacuum, ω the optical frequency of the SPP, and ϵ_m and ϵ_d are the dielectric constants of the metal and the dielectric, respectively. In order to excite SPPs with photons, the wavevector of the SPPs has to match the wavevector of the photons (phase matching). Since $\mathrm{Re}(\epsilon_m) < 0$ and $|\mathrm{Re}(\epsilon_m)| > \epsilon_d$, it is clear that $k_{SPP} > \omega/c\sqrt{\epsilon_d}$. Therefore, SPPs cannot be excited directly with photons incident from the dielectric. Three routes for SPP momentum matching exist: using a scatterer, grating coupling, or attenuated total reflection (ATR). In the first case, the scattering of, for instance, a subwavelength point, or line defect, provides the necessary uncertainty in k space to match the wavevector.[1] In the case of grating coupling, the grating constant can be added to the photon wavevector to match the wavevector of the SPP.[1]

We chose the third option: ATR. For this, the incident light travels through a different dielectric medium than the dielectric that will support the SPP.[22] This dielectric should have a dielectric constant $\epsilon_{d2} > \epsilon_d$, in our case a BK7-glass prism. The light propagating through the prism is incident on the metal-glass interface, with a wavevector component parallel to the metal surface, k_x, which is $k_x = \sqrt{\epsilon_{d2}}\omega/c \sin\theta$, where θ is the angle between the surface normal and incoming light. At the angle for total internal reflection at the glass-metal interface and larger, total internal reflection occurs, generating an evanescent tail of the incident light that will penetrate the metal. If the metal film is thin enough, the tail will reach the metal-air interface. Matching between the SPP k vector at the metal-air interface and the incoming photons can now be achieved by tuning θ. With this method, coupling efficiencies up to 90% are achievable. We chose this excitation scheme because the alternatives can cause a lot of unwanted scatter light. Also in ATR the SPP excitation is done from the opposite side of the sample than the detection site. This facilitates the design of the PSTM.

In order to couple the SPPs efficiently to micrometer-sized structures, the incoming light has to be focused down to a micrometer-sized spot using an objective. The angle of incidence no longer has a discrete value when using an objective but spans a range of angles, given by the numerical aperture (NA) of the objective. Therefore, not all incident light is coupled to SPPs. We found that with a NA of 0.3, a 30% coupling efficiency can be achieved.

II. MICROSCOPE REQUIREMENTS

In order to realize a microscope able to measure phase-sensitive and dynamical properties of propagating SPPs, the following requirements have to be fulfilled.

(1) Like all near-field microscopes, the vibration levels should be low enough to limit tip-sample variations due to environmental distortions to 1 nm peak-peak. They should preferably be even lower. This is because the near-field probe and sample have to be stable with respect to each other in order not to change the amplitude of the signal and to prevent damage to the probe.
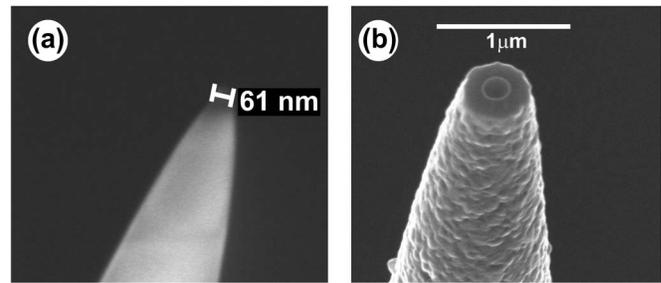

FIG. 1. (a) SEM micrograph of a typical near-field probe after pulling. The tip of the probe has a radius of 30 nm. (b) SEM micrograph of a typical coated near-field probe used for the experiments described in this paper. A probe like the one shown in (a) is coated with a 5 nm Cr adhesion layer and 200 nm Al. With a FIB a 200 nm aperture is fabricated.

(2) As will become clear in Sec. IV the complete setup needs to be temperature stabilized and shielded from air flows in order to minimize phase drift in the optical paths.
(3) The amplitude and phase of the SPPs should be detected as a function of position.
(4) The instrument should allow for time-resolved measurements of SPP propagation.
(5) The sample holder should be suitable to investigate plasmonic structures and therefore a prism for the ATR excitation should be mountable (see Sec. I A). The sample holder also needs to accommodate the investigation of photonic structures like photonic crystals, which requires coupling of light into the end facet of a photonic structure with either objective lenses or lensed fibers. As a result the sample should be accessible from all sides.
(6) A tip scanning microscope instead of a sample scanning microscope is desired. In a tip scanning microscope the sample will not move with respect to the laboratory frame which greatly facilitates incoupling of incident laser beams.
(7) In order to perform time-resolved measurements some sort of pump-probe configuration will be needed. We will show in Sec. V that for our measurements a delay line must be scanned with nanometer-size steps with a good reproducibility. A delay line with interferometric precision is therefore needed.

III. EXPERIMENTAL REALIZATION

The near-field probe forms a crucial part of a near-field microscope. Our probes are fabricated as follows. An optical fiber is pulled at both sides while a laser heats the fiber in the middle (Sutter instrument company, micropipette puller). As the fiber melts, it is pulled apart until it breaks, which results in two sharp tips at both sides. Under the proper heating and pulling conditions a tip with a radius of only a few tens of nanometers is obtained, combined with a sharp taper [see Fig. 1(a)]. To shield the probe from unwanted stray light, it is coated with a metal coating. With focused ion beam (FIB) milling, the end of the probe is polished, resulting in a flat end-facet with a roughness smaller than 10 nm and a well defined circular aperture. An important advantage of FIB treated probes is the reproducibility of the near-field optical

measurements.[23] All the measurements presented in this paper have been performed with a fiber probe that is coated with 200 nm of Al and 5 nm Cr as an adhesion layer. After FIB treatment, the apertures have a 100 nm radius, see Fig. 1(b).

As the tip of the probe is brought into the evanescent tail of a (propagating) E-field, e.g., of a SPP, a minute fraction of the evanescent tail is able to couple to the probe. Subsequently, this light is brought to a detector. The detector measures a signal proportional to the intensity of the E-field picked up by the probe which is, in the cases relevant to this paper, therefore proportional to the field inside the structure.

Because of the exponential decay of the evanescent field, the probe has to be within a few nanometers of the surface. Also we desire to measure the optical signal and the sample topography simultaneously, in order to be able to correlate the two. Two main techniques are possible: the first one is using atomic force microscopy in either contact mode or tapping mode,[24] and the second method is shear-force feedback.[25] We chose to work with shear-force feedback because with this technique there will be minimal contact between sample and probe and we avoid potential damage of the sample due to the probe. For shear-force feedback, a fiber, which ends in a near-field probe, is glued along the side of one of the prongs of a quartz tuning fork. The bare tuning fork has a resonance of $2^{15} = 32\,768$ Hz. Once a fiber is glued to the fork, the resonance of the fork is shifted a few hertz and the quality factor (Q) is reduced by several orders of magnitude to a typical value in the range of 200–700.[26] The tuning fork can either be dithered by an external piezoelement or driven electronically, which uses the piezoresponse of the quartz itself. We chose the first option because this configuration has the best signal-to-noise ratio.[27] By incorporating an oscillating tuning fork in one branch of an interferometer, we measured that for typical measurement conditions in our system, bending amplitudes are of the order of 1 nm. Because of this small movement and the detector integration time being two orders of magnitude longer than the dither frequency, we can ignore the prong movement on the optical signals for the remainder of the paper.

The externally driven prong movement in turn causes a measurable piezoelectric potential inside the quartz tuning fork, that is proportional to the tuning fork oscillation amplitude. Typically 10 nm above the surface, the probe-surface interaction becomes measurable. This interaction causes a shift in the resonance frequency and typically also extra damping of the tuning fork. Because the tuning fork is dithered with a constant frequency, the shift in resonance leads to a measurable change in the amplitude and phase of the piezoelectric potential produced by the quartz tuning fork. The change in phase with respect to the driving phase is measured and used to perform the height feedback.[28] When the probe is raster scanned over a sample, the feedback loop keeps the probe within the evanescent tail of the SPP. In this way, the time-averaged SPP intensity at different positions on the sample is measured. From the height-feedback signal the topography of the sample is simultaneously obtained with the optical signal.

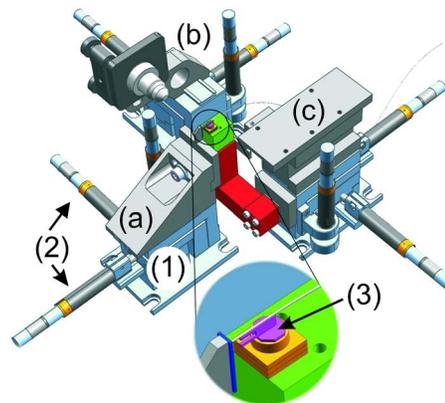In order to enable time-resolved measurements, an opti-

FIG. 2. (Color online) Sketch of the assembled microscope containing the sample holder, part (a), holding a sample (purple), illumination of the sample, part (b), and scanner mounting, part (c). All three parts are mounted on three-axis ULTRAlign™ positioning systems (1) including motorized stages (2). (The x-y probe scanner is shown in red and the z scanner in green). The tuning fork (pink) (3) is mounted on a steel base plate (pink) and fixed in position by a magnet (yellow). The tuning fork is dithered by a piezo shown (yellow).

cal delay line is added to the setup. To obtain a feedback motion on the position of the delay line a Heidenhain LIP 372 exposed linear encoder is used. This encoder obtains its position information by counting the individual increments of a periodic structure. It can measure a total travel of 70 mm. The actual motion is achieved with a PI M-014.DP1 translation stage and a M-227.25 dc actuator, with a 25 mm travel combined with a PI P-840.30 piezoactuator, which has a 45 μm travel and enabling 3.5 nm resolution of the complete system. While scanning the optical delay line, the piezoactuator will take 3.5 nm steps until it reaches its maximum range. At maximum range, the dc actuator travels 45 μm and the piezo shrinks back correspondingly to its minimum extension. This mode of operation results in a caterpillar-like movement. The linear encoder meanwhile monitors the movement and corrects for deviations from the desired movement.

A. Sample holder and scanner mount

We chose to mount the sample at right angles to the optical table and designed the sample mount accordingly, see Fig. 2. Thus, we obtain full flexibility in the excitation direction since the sample is easily accessible from all angles in the horizontal plane, and we have enough space for the ATR excitation. This way of mounting fixes only one side of the holder with respect to the scanner. It is a less stable solution than in the case of a sample mounted parallel to the optical table and fixed at three or four sides. Although this choice of sample mounting is expected to give rise to vibrational instabilities, we will show in this section that it is possible to obtain the required stability.

The sample holder needs to be as compact and stable as possible. The 561/562 series ULTRAlign™ precision multi-axis positioning system from Newport is able to meet the desired stability. Sample holder and stage are connected to each other by the use of an Al bridge. The ULTRAlign™ positioning system is also used as a base for the sample
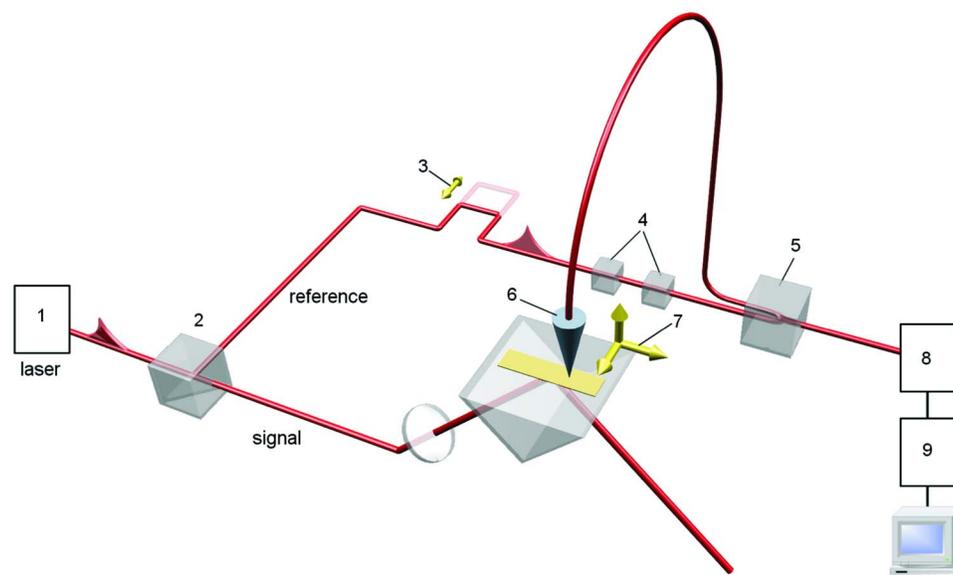
FIG. 3. (Color online) Sketch of the complete setup. In (1) a laser system produces femtosecond pulses that are split by a beam splitter (2). Inside the reference branch a delay line (3) and two AO modulators (4) are incorporated. SPPs are excited in the signal branch and picked up by the probe (6) that is actuated in the x, y, and z directions (7). The signals from the reference branch and signal branch are mixed (5) and the interference signal is collected by a detector in (8). A lock-in detector (9) processes the detector signal and sends it to a PC.

holder. Instead of manual spindles, motorized actuators are used for the positioning. The probe approach to the sample is automated using similar motors on the positioning system that holds the scanner. In the automized approach a feedback loop monitors the tuning fork signal to stop the motor-controlled stage movement as soon as a shear force is detected between the near-field probe and the sample surface. The approach is performed with a speed of 2 μm/s and gives a 100% successful approach (excluding human errors). Figure 2 shows in light blue (1) the ULTRAlign™ positioning systems on which the sample holder (a) is mounted, containing in dark blue the sample, an objective for illumination (b), and the scanner (c). The motorized actuators are indicated by (2).

Mounted on the positioning system is a Piezo Jena series PXY 200 D12 scanner for probe scanning (red part in Fig. 2). It has a 200 μm range in two directions and was customized with an extra thick housing for more vibrational stability. For the z motion we chose the PZ 20 D12, also from Piezo Jena. The actuator yields an 8 μm range in the direction perpendicular to the sample (green part in Fig. 3). To connect the tuning fork to the scanner, the tuning fork is soldered on a 0.5×0.5 cm^2 steel plate. The plate is in turn fixed in place on the z piezo with a magnet. In the magnified section of Fig. 2 the tuning fork and steel plate are depicted in pink (3). In the same part of the figure the magnet and dither piezo are shown in yellow. The dither piezo is fixed in between the z piezo and the magnet to excite the tuning fork mechanically. The piezoelectric potential from the quartz tuning fork is amplified by a 100 times preamplifier, positioned roughly 2 cm from the tuning fork. The amplified signal is fed into the electronic height-feedback loop. In a real measurement situation it is possible to scan with a scan speed of the order of 20 μm/s containing 50 nm steps for two weeks nonstop without crashing the probe into the sample.

The complete system is shown in Fig. 3. The light path starts with the laser system (1), which generates femtosecond laser pulses. These pulses are split by a beam splitter (2). The necessity for the two branches will be made clear in Sec. IV

as the scheme for phase-sensitive measurements is described. The reference branch consists of a delay line (3) and the two acoustic-optic (AO) modulators (4). It ends at the mixing point (5). In the signal branch SPPs are excited and detected by the near-field probe (6). The probe is scanned in the x-y plane and kept at a constant height above the sample surface in the z direction so that a height contour of in the sample surface is obtained (7). The E-field in the signal branch and the E-field in the reference branch interfere in the mixing point (5). The interference is collected by a detector (8). The detector signal is fed to a lock-in amplifier (9), of which the output is sent to a personal computer (PC).

B. Microscope stability

The complete apparatus is built on an optical table which is passively damped. The complete setup, excluding the electronics and laser system, is enclosed by a box to isolate the optical paths from temperature differences and air drift. Figure 4 shows the vibrational spectrum as measured on the
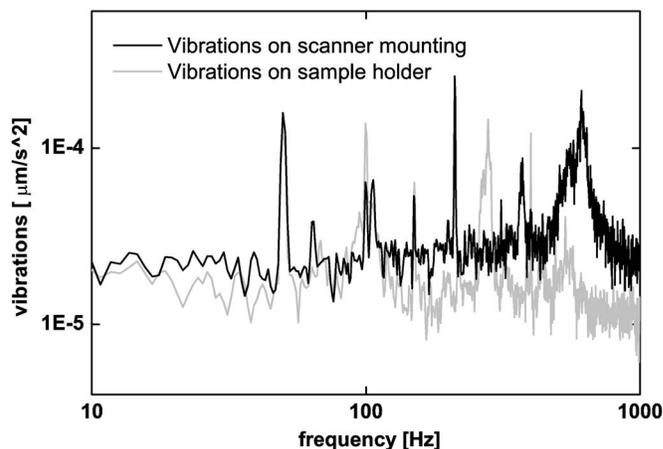

FIG. 4. Spectrum of the vibrations on the sample holder [(a) in Fig. 2] and scanner mounting [(c) in Fig. 2], measurement with a calibrated accelerometer during representative experimental conditions. The near-field probe is scanned over the surface and the height control is activated.
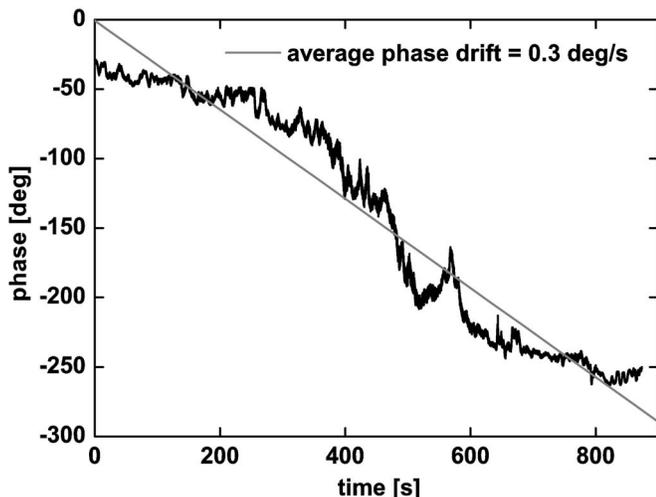
FIG. 5. Measurement of the phase drift in the system. For this measurement the near-field probe was kept at a fixed position above a reference waveguide, and the phase information of an E-field inside the guide is monitored in time. From the linear fit we obtain an average phase drift of $0.3°/s$.

sample holder [(a) in Fig. 2] and scanner mounting [(c) in Fig. 2] under standard measurement conditions, i.e., the probe is scanning and kept within a few nanometers of the surface by the shear-force feedback. Vibrations were measured by placing a calibrated accelerometer (bandwidth: 1 Hz) on both the sample holder and scanner mount. The accelerometers were positioned to measure accelerations perpendicular to the sample surface, which is the most important direction for minimizing vibrations in any scanning probe microscope. Clear resonances are observed in the vibration measurements. However, all of them have accelerations that are orders of magnitude lower than those required for typical commercial scanning electron microscopes. None of the resonances appear in both measurement series, which indicates that the passively damped optical table filters out all vibrations coming from the laboratory environment. Of the resonances at 50 and 100 Hz, visible in both spectra, it has been determined that they are the result of unwanted cross-talk between the mains and the electronics of the accelerometer.

To quantify the phase drift in the microscope we performed a measurement in which we monitor the phase in a reference waveguide, which is described in Sec. VI A. The phase of the E-field at the position of the probe is monitored over time in a way that will be described in detail in Sec. IV. Figure 5 shows the result of the phase drift measurement which shows an average phase drift of only $0.3°/s$. This drift is due to a small temperature drift in the laboratory environment and forms an upper limit. Under typical measurement conditions the phase drift will show a random walk around an average phase.

C. Electronics

The electronic part of the height-feedback loop is schematically depicted in Fig. 6. During operation the tuning fork (1) is dithered by a piezo driven at the tuning fork resonance by a function generator. The tuning fork typically produces a piezoelectric potential in the order of 1 mV. This is amplified by an amplifier and send to a bandpass module (bandwidth in the order of 1 kHz), which filters around the tuning fork resonance frequency. The phase module determines the phase difference between the filtered signal from the tuning fork and a reference phase from the function generator. In the feedback module, the measured phase difference is compared to a manually set reference phase. With this reference phase, the amount of interaction between sample and probe is set. The feedback module yields a feedback signal that is amplified by a high voltage amplifier and is finally sent to the z piezo to control the probe height, thereby completing the feedback loop.

IV. A PHASE-SENSITIVE PSTM

In order to obtain phase-sensitive near-field measurements, we have incorporated the microscope in a (Mach-Zehnder) interferometer.[24,29–32] Hereto, the light from a laser source is split into two beams to form the branches of the interferometer. One beam is directed to the sample to excite
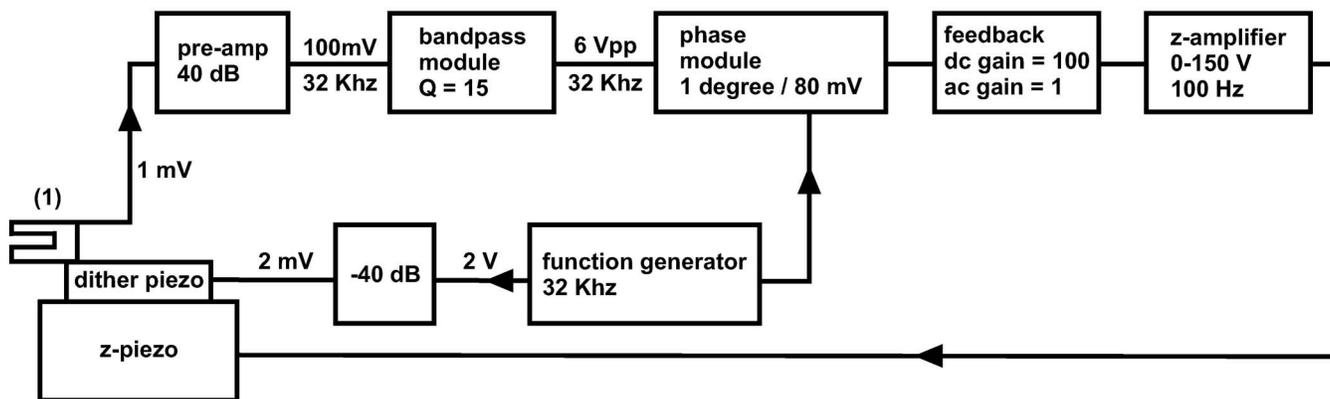

FIG. 6. Diagram of the feedback loop used for the shear-force height feedback. At (1) a tuning fork is dithered by a piezo driven by a function generator. It produces a piezoelectric potential that is amplified by a preamplifier and sent to a bandpass filter module. The phase of this signal is extracted in a phase module and compared to a reference phase from the function generator. A feedback module compares the phase from the phase module to a manual set reference phase and provides a feedback signal that is amplified by a high voltage amplifier and sent to the z piezo. The piezo actuates the probe perpendicular to the sample surface, thus completing the feedback loop.

SPPs. A fraction of the E-field is picked up by the near-field probe and brought to the mixing point of the interferometer. This branch (including beam splitter to sample path, propagation in sample, and pickup fiber) is called the signal branch. The other beam is called reference branch and contains an optical delay line and two acousto-optic modulators to shift the optical frequency.

The following description of the phase-sensitive PSTM is valid for any photonic structure. However, from this point on we will consider the case of SPP detection only for clarity. The fraction of the SPP E-field that is picked up by the near-field probe in the signal branch, $E_{\text{sig}}(x,y)$, can be described in the following way when continuous wave (cw) excitation is used:

$$E_{\text{sig}}(x,y,t) = A_{\text{sig}}(x,y)\exp\{i[\omega t + \phi_{\text{sig}}(x,y)]\}. \quad (2)$$

Here $A_{\text{sig}}(x,y)$ is the amplitude of the E-field picked up at position (x,y), ω the frequency of the laser used to excite the SPPs, and $\phi_{\text{sig}}(x,y)$ the phase of the SPP E-field.

The optical frequency of the light inside the reference branch is shifted by 40 kHz by using two traveling-wave acoustic-optical modulators (AO modulators), which shift the optical frequency in their diffracted orders without introducing a time-dependent amplitude. One of the AO modulators is driven at 80.04 MHz, and the other is driven at 80.00 MHz. The +1st diffraction order of the first AO modulator is incident on the second AO modulator of which the −1st order is used in the rest of the reference branch, resulting in the desired frequency shift of 40 kHz. The E-field in the reference branch E_{ref} is described as follows:

$$E_{\text{ref}}(t) = A_{\text{ref}} \exp\{i[(\omega + \Delta\omega)t + \phi_{\text{ref}}]\}. \quad (3)$$

Here, $\Delta\omega$ is the 40 kHz frequency shift, A_{ref} is the amplitude of the E-field in the reference branch, and ϕ_{ref} is the phase of the E-field in the reference branch. At the mixing point E_{sig} and E_{ref} will interfere. The interference signal is detected and the detector measures intensity, I_{det}:

$$
\begin{aligned}
I_{\text{det}}(x,y,t) &\propto |E_{\text{sig}}(x,y,t) + E_{\text{ref}}(t)|^2 \\
&= A_{\text{sig}}(x,y)^2 + A_{\text{ref}}^2 + 2A_{\text{sig}}(x,y)A_{\text{ref}}\cos[\Delta\omega t \\
&\quad + \phi(x,y)],
\end{aligned} \quad (4)
$$

with $\phi(x,y)$ the effective phase difference between signal and reference branch $[\phi_{\text{ref}} - \phi_{\text{sig}}(x,y)]$. The detector signal is fed into a lock-in amplifier (LIA) which discards the dc terms, and effectively multiplies the remaining with $\cos(\Delta\omega t)$. Subsequently, it integrates over a set time T, much longer than $1/\Delta\omega$, i.e., $T > 2,5 \times 10^{-5}$ s in our case. In the measurements presented in this paper $T = 1 \times 10^{-3}$ s was chosen. After the integration we are left with an intensity measured by the lock-in $I_{\text{LIA,1}}$:

$$
\begin{aligned}
I_{\text{LIA,1}}(x,y) &\propto \frac{1}{T}\int_0^T [\cos(\Delta\omega t)]\{2A_{\text{sig}}(x,y)A_{\text{ref}}\cos[\Delta\omega t \\
&\quad + \phi(x,y)]\}dt \\
&\propto \frac{2A_{\text{sig}}(x,y)A_{\text{ref}}}{T}\int_0^T \left[\frac{1}{2}\cos\phi(x,y)\right.
\end{aligned}
$$

$$
\left. + \frac{1}{2}\cos[2\Delta\omega t + \phi(x,y)]\right]dt
$$

$$
\propto A_{\text{sig}}(x,y)A_{\text{ref}}\cos[\phi(x,y)]. \quad (5)
$$

The LIA also produces a signal that is shifted by 90°:

$$I_{\text{LIA,2}}(x,y) \propto A_{\text{sig}}(x,y)A_{\text{ref}}\sin[\phi(x,y)]. \quad (6)$$

These two results, Eqs. (5) and (6), are the two outputs of the lock-in amplifier. They can be combined to obtain a signal I_{SPP} at the measurement position:

$$
\begin{aligned}
I_{\text{SPP}}(x,y) &\propto \langle\{A_{\text{sig}}(x,y)A_{\text{ref}}\cos[\phi(x,y)]\}^2 \\
&\quad + \{A_{\text{sig}}(x,y)A_{\text{ref}}\sin[\phi(x,y)]\}^2\rangle^{1/2} \\
&\propto A_{\text{sig}}(x,y)A_{\text{ref}}. \quad (7)
\end{aligned}
$$

Since the amplitude in the reference branch is constant, I_{SPP} is proportional to the *amplitude* of the SPP E-field at position (x,y). The phase of the SPP E-field relative to a (constant) reference phase ϕ_{ref} is given by

$$\phi_{\text{SPP}}(x,y) = \arctan\frac{A_{\text{sig}}(x,y)A_{\text{ref}}\sin[\phi(x,y)]}{A_{\text{sig}}(x,y)A_{\text{ref}}\cos[\phi(x,y)]}. \quad (8)$$

Note that this $\phi_{\text{SPP}}(x,y)$ may contain a possible phase drift in one or both optical branches due to temperature changes and/or other environmentally induced drifts. The influence of this drift is discussed in Sec. III B.

Heterodyne detection has another advantage besides phase information: it also increases the system's sensitivity. In a conventional experiment one measures

$$I_s \propto |A_{\text{sig}}|^2. \quad (9)$$

Since $I_{\text{SPP}} \propto A_{\text{sig}}(x,y)A_{\text{ref}}$, the heterodyne detection results in a signal enhancement of $A_{\text{ref}}/A_{\text{sig}}$. Since the amplitude inside the reference branch can be made orders of magnitude higher than the signal picked up by the probe, this easily gives a factor of >10 signal-to-noise enhancement in real measurement situations. This means that signals in the order of femtowatts are detectable.

By raster scanning the probe above a waveguide guiding SPPs $A_{\text{SPP}}(x,y)$ and $\phi_{\text{SPP}}(x,y)$ are measured at different positions. The setup described above will in this case measure a time-averaged E-field distribution, containing the phase information.

V. AN ULTRAFAST PSTM

The investigation of SPP dynamics uses (femtosecond) laser pulses instead of a cw laser. The limited coherence length of the optical pulse will only result in interference between the pulse in the reference branch and the pulse in the signal branch if they have time overlap on the detector. Thus time-resolved measurements become possible.[33] The group velocity dispersion (GVD) in the signal and reference branches was balanced because an imbalance in GVD will reduce the amplitude of the interference signal.[34] The dispersion of the sample is intentionally not balanced because it is of scientific interest. Two measurement schemes for studying SPP dynamics are possible. In one scheme, the reference branch is fixed in length, and the probe is raster scanned over the surface. Subsequently, the reference branch is made

longer or shorter and the measurement is repeated. This scheme is described in Sec. V A. Alternatively, the probe can be fixed in space with respect to the sample, and the reference branch can be made longer or shorter. This measurement is repeated at different positions of the near-field probe. Section V B describes this scheme in more detail.

A. Measurement scheme 1: Fixed time, scanning probe

In order to describe a measurement using femtosecond pulses extra time dependencies have to be introduced in Eqs. (2) and (3):

$$E_{sig}(x,y,t) = A_{sig}(x,y,t)\exp\{i[\omega t + \phi_{sig}(x,y)]\}, \quad (10)$$

$$E_{ref}(t-\tau) = A_{ref}(t-\tau)\exp\{i[(\omega + \Delta\omega)(t-\tau) + \phi_{ref}]\}, \quad (11)$$

with τ a time delay between the two branches. The analysis used in Sec. IV yields

$$I_{LIA,1}(x,y) \propto \cos[\phi(x,y)]\int_0^T A_{sig}(x,y,t)A_{ref}(t-\tau)dt \quad (12)$$

and

$$I_{LIA,2}(x,y) \propto \sin[\phi(x,y)]\int_0^T A_{sig}(x,y,t)A_{ref}(t-\tau)dt. \quad (13)$$

The intensity measured by the LIA will be proportional to the interference integral between the amplitudes in the two branches. For a detailed description of femtosecond pulse tracking see Ref. 34. If one now raster scans the probe above a propagating SPP wavepacket, the position of the probe will determine the length of the signal branch. This way a image that resembles a snapshot of the propagating SPP pulse in space is visualized for a given time.

B. Measurement scheme 2: Fixed probe position, scanning time

Alternatively, we can fix the near-field probe at a position (x,y) with respect to the sample. This means that ϕ_{sig} and ϕ_{ref} will be constant with respect to each other. Therefore we neglect all phase terms in the following description. Again, E_{ref} will depend on time t with a delay time τ set by a delay line. This means that the E-fields inside the signal and reference branches can be written as

$$E_{sig}(t) = A_{sig}(t)\exp\{i\omega t\} \quad (14)$$

and

$$E_{ref}(t-\tau) = A_{ref}(t-\tau)\exp\{i(\omega + \Delta\omega)(t-\tau)\}, \quad (15)$$

respectively.

In this configuration the intensity at the detector will be

$$I_{det}(t-\tau) = A_{sig}(t)^2 + A_{ref}(t-\tau)^2 + 2A_{ref}(t-\tau)A_{sig}(t)$$
$$\times \cos(-\omega\tau + \Delta\omega t - \Delta\omega\tau), \quad (16)$$

which yields for the output of the lock-in amplifier:

$$I_{LIA}(t-\tau) \propto \frac{1}{T}\int_0^T [\cos(\Delta\omega t)][2A_{sig}(t)A_{ref}(t-\tau)$$
$$\times \cos(-\omega\tau + \Delta\omega t - \Delta\omega\tau)]dt. \quad (17)$$

For the simplest case of a Gaussian pulse and no dispersion during propagation in the signal branch, this equation can be evaluated as

$$I_{LIA}(\tau) \propto \frac{2}{T}\int_0^T A_{sig}(t)A_{ref}(t-\tau)dt\int_0^T \frac{1}{2}\cos(\Delta\omega t - \tau\{\omega$$
$$+ \Delta\omega\})dt \propto \frac{1}{2\sqrt{\pi}}\exp\left(-\frac{\tau^2}{4}\right)\cos(\tau\{\omega + \Delta\omega\}). \quad (18)$$

$\Delta\omega$ (40 kHz) is orders of magnitude smaller than the optical frequency of the laser ($\omega \approx 200$ THz) and is therefore neglected in the remainder of this analysis for clarity. For this simplification the two LIA outputs will be

$$I_{LIA,1}(\tau) \propto \frac{1}{2\sqrt{\pi}}\exp\left(-\frac{\tau^2}{4}\right)\cos(\tau\omega) \quad (19)$$

and

$$I_{LIA,2}(\tau) \propto \frac{1}{2\sqrt{\pi}}\exp\left(-\frac{\tau^2}{4}\right)\sin(\tau\omega), \quad (20)$$

respectively. It is easy to see now that I_{LIA} will be maximum if the two branches are equal in length, i.e., $\tau=0$.

Equations (19) and (20) differ from Eqs. (12) and (13) in the sense that in the previous measurement scheme there was a dependency on position (x,y) since the near-field probe was scanned. If the SPP propagates through a dispersive medium, the interference between the signal and reference branch will be influenced by this dispersion.[34] In this measurement scheme the influence of dispersion is smaller than in the previous one.

For a real measurement situation there will be dispersion in the SPP guide, and we have to write the integral in Eq. (17) as a multiplication in the Fourier domain:

$$I_{LIA}(\tau) \propto \frac{1}{T}\int_0^T E_{sig}(t)E_{ref}^*(t-\tau)dt \propto \mathcal{F}^{-1}[E_{sig}(\omega)E_{ref}^*(\omega)], \quad (21)$$

see also Ref. 35. This result shows another difference between this measurement scheme and the previous one: the Fourier transform of I_{LIA} gives a signal that is proportional to the product of the optical spectrum of the SPP and the (known) spectrum of the pulse in the reference branch.

VI. RESULTS

To show that the designed near-field microscope meets all the requirements as stated in Sec. II we performed two measurements. We start with a ridge waveguide that was studied in detail[30] as a reference to prove that the microscope works and is phase sensitive. By studying this waveguide with this setup we show that the microscope is not only capable of measuring SPPs but also supports end-fire coupling for photonic systems. In Sec. VI B we turn to a SPP
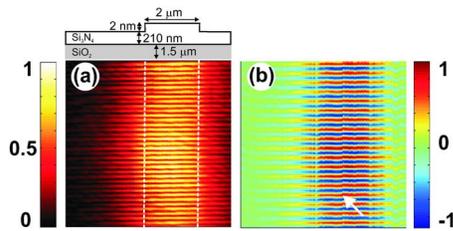
FIG. 7. (Color online) (a) Normalized amplitude measurement of the E-field inside a 2 μm wide, 212 nm high waveguide, incident wavelength cw and 632.8 nm. Scan frame is 6.3 μm^2, scan direction from top to bottom. Above the measurement frame a schematic of the waveguide is shown. White lines indicate the edges of the waveguide in the measurement frame. A periodicity of 180 nm is observed, which indicates a standing wave inside the guide. Also a 10 μm beating is barely visible, which is caused by a spatial mode beating between TE and TM modes. (b) Normalized amplitude times $\cos(\phi)$ of the E-field of the same area measured simultaneously with (a). Individual phase fringes are resolved, which have a periodicity of 360 nm. The white arrow indicates a phase shift due to phase drift in one of the optical branches.

waveguide. For this guide we prove that the microscope is able to measure SPPs phase sensitive and ultrafast as was required.

A. Measurements on a photonic model system

The photonic model system consists of a 2 μm wide Si$_3$N$_4$ waveguide on top of thermal silicon oxide. The height of the Si$_3$N$_4$ layer is 210 nm and a ridge step of 2 nm is created to form the waveguide. A schematic of the waveguide is shown above Fig. 7(a). Figure 7 shows the measurement results when cw HeNe-laser light (free space wavelength=632.8 nm) is coupled into the waveguide. The total scan range of this measurement is 6.3 $\times$ 6.3 μm^2. In the amplitude image [Fig. 7(a)], the time-averaged, normalized amplitude of the E-field inside the guide is shown. White lines indicate the edges of the guide. The E-field is confined to the guide and two amplitude beating patterns are visible. One has a period of 180 nm and one has a periodicity of 10 μm (obtained from a different measurement with a longer scan range). The fast beating indicates an amplitude modulation with a period of half the wavelength, which is caused by the interference between the incident mode and light reflected back at the end of the guide. The slower beating turns out to be spatial mode beating between TE and TM polarized modes. In the normalized phase and amplitude picture, Fig. 7(b), measured simultaneously with Fig. 7(a), individual phase fringes are resolved. Now a clear periodicity of 360 nm is observed which is twice the period observed in the amplitude image [Fig. 7(a)]. The measured period is in good agreement with the 352 nm wavelength calculated for the TE mode in the guide. It is clear in Fig. 7(b) that two consecutive areas of high amplitude in Fig. 7(a) have a different phase, which causes the period to become twice as long, allowing a direct observation of the wavelength inside the photonic structure. Please note that the phase in every high-amplitude area is not constant as is expected for a standing wave. This is caused by the fact that the amplitude of the incoming light is higher than that of the reflected light. Hence, the incoming light dominates the phase evolution of the light inside the waveguide.
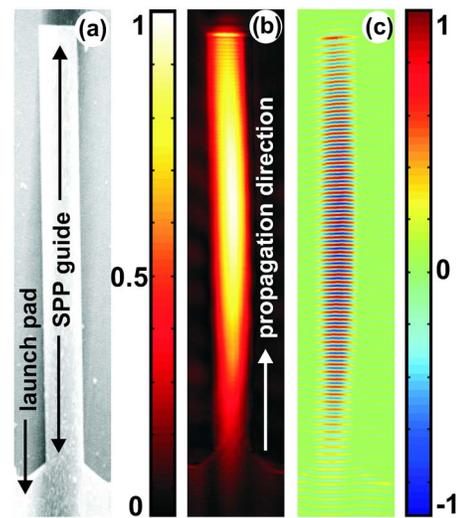

FIG. 8. (Color online) (a) Topography of the SPP waveguide obtained by shear-force feedback. It consists of a 55 nm thick Au guide, 6 μm wide and 80 μm long. (b) Normalized amplitude measurement of the E-field of the SPP wavepacket inside the 6 μm waveguide. (c) Combined phase and amplitude information [$\sim A \cos(\phi)$] of the same measurement as (b). Scan lines run from top to bottom and the scan frame is 15 $\times$ 110 μm^2, wavelength in air used to excite the SPPs: 1500 nm pulses with 20 nm bandwidth.

B. Measurements on a SPP waveguide

We performed ultrafast and phase-sensitive measurements of SPPs guided by a straight SPP guide. We used the scheme in which we scan the probe and keep the delay line fixed (the scheme described in Sec. V A). In Fig. 8(a) the topography of the SPP structure under investigation obtained by the shear-force feedback is shown. The guide, a 55 nm thick Au stripe, was prepared lithographically on a glass substrate such that a 6 μm wide Au stripe protrudes from a launch pad. Part of this launch pad is visible in the bottom of Fig. 8(a). The total length of the guide is 80 μm. SPPs are excited using the ATR configuration at the gold-air interface of the launch pad using a Ti:sapphire laser pumped optical parametric oscillator (pulse duration of 120 fs, repetition rate of 80 MHz, wavelength in air of 1500 nm, and bandwidth of 30 nm). As femtosecond pulses are used to excite the SPPs, femtosecond SPP wavepackets are created.

In Fig. 8(b) we show the normalized amplitude information of the SPP E-field. The probe is scanned from top to bottom of the figure (scan frame of 15 $\times$ 110 μm^2) and the recording of one frame takes approximately 30 min measuring time. At the end of the guide SPPs are scattered into photons, and part is reflected back forming a standing wave pattern visible in the top of the guide. The SPP is strongly confined inside the 6 μm Au guide and only a single mode is excited. Theoretical predictions[36] expect that a 6 μm wide guide for the wavelength used should just be able to support two modes. Apparently we only excite one, since no mode beating can be observed. The full width at half of the maximum amplitude of length of the SPP wavepacket is 73$\pm$1 μm, which is in good agreement with the theoretically expected 72 μm, based on a 120 fs pulse.

Figure 8(c) shows the normalized amplitude multiplied by the cosine of the phase of the propagating SPP wavepacket. From this measurement the SPP wavevector is di-
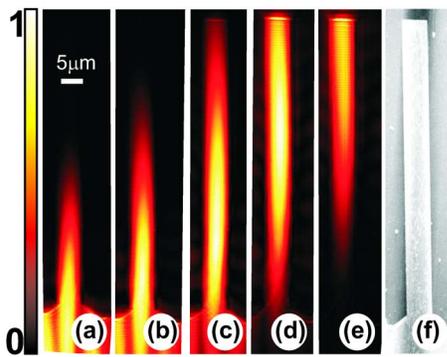
FIG. 9. (Color online) (a)–(e) Normalized amplitude information of the SPP wavepacket E-field. Succeeding frames are new scans of the probe. In between the frames the delay line is lengthened to 14.4 μm. Therefore, the time between two frames is 48 fs. The scan frame is 15×110 μm^2, scan lines run from top to bottom. (f) Topography of the SPP waveguide obtained by shear-force feedback.

rectly obtained by measuring the periodicity of the phase fringes. The SPP wavevector is approximately 4.1 $\times 10^{-3}$ nm^{-1}, which is roughly 1.02 times the vacuum wavevector of the light used to excite the SPPs. This means that the SPPs are extremely photonlike, but still bound to the Au-air interface.

C. Time-resolved measurements on SPPs

When the SPP wavepacket is probed for different settings of the optical delay line, we visualize the wavepacket at different positions in time as it propagates along the guide [Figs. 9(a)–9(e)]. Every frame is a new scan of the measurement frame, scan direction again from top to bottom of the figure. The time delay between each frame is determined by the displacement of the delay line of 7.2 μm, corresponding to 48 fs. From this measurement sequence we can study the SPP dynamics in a direct way. Two properties that follow directly from this measurement are SPP group velocity, by following the wavepacket in time, and its amplitude attenuation length, by looking at the decay of the SPP as it propagates, they are 2.5×10^8 m/s and 70 μm, respectively. This amplitude attenuation length corresponds to an intensity attenuation length of 35 μm.

For the measurement described above, measurement scheme 1 was used, see Sec. V A. Figure 10 shows the result when measurement scheme 2 (see Sec. V B) is used at the same structure. The near-field probe is fixed at the entrance of the SPP guide and the delay line is scanned. The result is a cross-correlation between the wavepacket in the reference branch and the SPP wavepacket.

VII. CONCLUSIONS

In the following we will show that all requirements stated in Sec. II have been met.

(1) The stability of the microscope is discussed in Sec. III B and turned out to be good enough to measure two weeks nonstop in which the near-field probe maintained within 10 nm of the sample without observable damage to the probe. Also it was possible to observe 2 nm steps in sample topography.
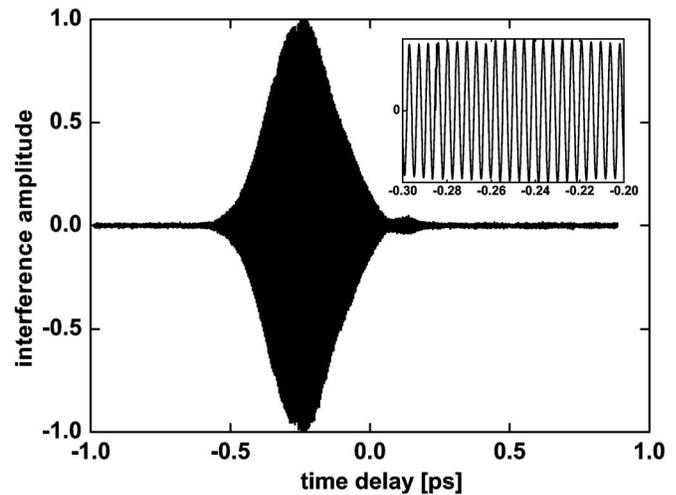

FIG. 10. Typical measurement using measurement scheme 2 (see Sec. V B). The probe is fixed with respect to the sample and the delay line is scanned. In this measurement the probe was fixed at the beginning of the guide used for the measurements described in Sec. VI A. Inset is a zoom in on the center of the interferogram.

(2) In Sec. VI A we showed that the phase drift in the interferometer is $0.3°$/s, which is small enough to perform stable measurements.
(3) In Sec. III we showed that it is possible to measure the amplitude and phase of (guided) SPPs.
(4) Time-resolved measurements on (guided) SPPs have been obtained and shown in Sec. VI C.
(5) In Sec. VI A we showed that the microscope is also compatible with photonic waveguides.
(6) The realized microscope is tip scanning and has a scan range of 200×200 μm^2 as desired.
(7) In Sec. III A a delay line with interferometric precision is described as was desired and in Fig. 10 it was shown that the delay line can be scanned with the desired position.

Also the basics of near-field microscopy are discussed in this paper, and the necessary adaptations for time- and phase-resolved measurements are presented. This instrument enables ultrafast investigations of SPP dynamics in metallic nanostructures, of photonic crystal structures, and of components for integrated optical circuits.

ACKNOWLEDGMENTS

[1] H. Raether, *Surface Plasmons on Smooth and Rough Surfaces and on Grating* (Springer, Berlin, 1986).
[2] W. L. Barnes, A. Dereux, and T. W. Ebbesen, Nature (London) **424**, 824

(2003).

[3] E. Ozbay, Science **311**, 189 (2003).

[4] G. Gbur, H. F. Schouten, and T. D. Visser, Appl. Phys. Lett. **87**, 191109 (2005).

[5] I. I. Smolyaninov, J. Elliott, A. V. Zayats, and C. C. Davis, Phys. Rev. Lett. **94**, 057401 (2005).

[6] D. Derkacs, S. H. Lim, P. Matheu, W. Mar, and E. T. Yu, Appl. Phys. Lett. **89**, 093103 (2006).

[7] A. D. McFarland and R. P. Van Duyne, Nano Lett. **3**, 1057 (2003).

[8] J. Homola, Anal. Bioanal. Chem. **377**, 528 (2003).

[9] B. Hecht, H. Bielefeldt, L. Novotny, Y. Inouye, and D. W. Pohl, Phys. Rev. Lett. **77**, 1889 (1996).

[10] H. Ditlbacher, J. R. Krenn, N. Felidj, B. Lamprecht, G. Schider, M. Salerno, A. Leitner, and F. R. Aussenegg, Appl. Phys. Lett. **80**, 404 (2002).

[11] E. Verhagen, A. L. Tchebotareva, and A. Polman, Appl. Phys. Lett. **88**, 121121 (2006).

[12] H. H. Rotermund, Surf. Sci. Rep. **29**, 267 (1997).

[13] A. Kubo, K. Onda, H. Petek, Z. Sun, Y. S. Jung, and H. K. Kim, Nano Lett. **5**, 1123 (2005).

[14] A. Kubo, N. Pontius, and H. Petek, Nano Lett. **7**, 470 (2007).

[15] M. van Exter and A. Lagendijk, Phys. Rev. Lett. **60**, 49 (1988).

[16] E. Betzig, J. K. Trautman, T. D. Harris, J. S. Weiner, and R. L. Kostelak, Science **251**, 1468 (1991).

[17] I. I. Smolyaninov, W. Atia, and C. C. Davis, Phys. Rev. B **59**, 2454 (1999).

[18] J.-C. Weeber, J. R. Krenn, A. Dereux, B. Lamprecht, Y. Lacroute, and J. P. Goudonnet, Phys. Rev. B **64**, 045411 (2001).

[19] J.-C. Weeber, Y. Lacroute, and A. Dereux, Phys. Rev. B **68**, 115401

(2003).

[20] R. Zia, J. A. Schuller, A. Chandran, and M. L. Brongersma, Mater. Today **9**, 20 (2006).

[21] H. L. Offerhaus, B. van den Bergen, M. Escalante, F. B. Segerink, J. P. Korterik, and N. F. van Hulst, Nano Lett. **5**, 2144 (2005).

[22] E. Kretschmann and H. Z. Raether, Z. Naturforsch. A **23**, 2135 (1968).

[23] J. A. Veerman, A. M. Otter, L. Kuipers, and N. F. van Hulst, Appl. Phys. Lett. **72**, 3115 (1998).

[24] R. Hillenbrand and F. Keilmann, Phys. Rev. Lett. **85**, 3029 (2000).

[25] E. Betzig, P. L. Finn, and J. S. Weiner, Appl. Phys. Lett. **60**, 2484 (1992).

[26] K. Karrai and R. D. Grober, Appl. Phys. Lett. **66**, 1842 (1995).

[27] C. L. Jahncke, O. Brandt, K. E. Fellows, and H. D. Hallen, Rev. Sci. Instrum. **75**, 2759 (2004).

[28] A. G. T. Ruiter, J. A. Veerman, K. O. van der Werf, and N. F. van Hulst, Appl. Phys. Lett. **71**, 28 (1997).

[29] M. Vaez-Iravani and R. Toledo-Crow, Appl. Phys. Lett. **62**, 1044 (1993).

[30] M. L. M. Balistreri, J. P. Korterik, L. Kuipers, and N. F. van Hulst, Phys. Rev. Lett. **85**, 294 (2000).

[31] I. Stefanon, S. Blaize, A. Bruyant, S. Aubert, G. Lerondel, R. Bachelot, and P. Royer, Opt. Express **13**, 5553 (2005).

[32] A. Nesci, R. Dändliker, and H. P. Herzig, Opt. Lett. **26**, 208 (2001).

[33] M. L. M. Balistreri, H. Gersen, J. P. Korterik, L. Kuipers, and N. F. van Hulst, Science **295**, 1080 (2001).

[34] H. Gersen, J. P. Korterik, N. F. van Hulst, and L. Kuipers, Phys. Rev. E **68**, 026604 (2003).

[35] R. J. P. Engelen, Y. Sugimoto, Y. Watanabe, J. P. Korterik, N. Ikeda, N. F. van Hulst, K. Asakawa, and L. Kuipers, Opt. Express **14**, 1658 (2006).

[36] R. Zia, M. D. Selker, and M. L. Brongersma, Phys. Rev. B **71**, 165431 (2005).